



Kill three birds with one stone: Mitochondria-localized tea saponin derived carbon dots with AIE properties for stable detection of HSA and extremely acidic pH

Shengtao Zhang, Bin Li, Jieyu Zhou, Jiayi Shi, Zhongjing He, Yumin Zhao,
Yan Li, Yehua Shen, Yongmin Zhang, Shaoping Wu

► To cite this version:

Shengtao Zhang, Bin Li, Jieyu Zhou, Jiayi Shi, Zhongjing He, et al.. Kill three birds with one stone: Mitochondria-localized tea saponin derived carbon dots with AIE properties for stable detection of HSA and extremely acidic pH. Food Chemistry, 2023, 405, pp.134865. 10.1016/j.foodchem.2022.134865 . hal-03855738

HAL Id: hal-03855738

<https://hal.sorbonne-universite.fr/hal-03855738>

Submitted on 16 Nov 2022

HAL is a multi-disciplinary open access archive for the deposit and dissemination of scientific research documents, whether they are published or not. The documents may come from teaching and research institutions in France or abroad, or from public or private research centers.

L'archive ouverte pluridisciplinaire **HAL**, est destinée au dépôt et à la diffusion de documents scientifiques de niveau recherche, publiés ou non, émanant des établissements d'enseignement et de recherche français ou étrangers, des laboratoires publics ou privés.

Kill three birds with one stone: Mitochondria-localized tea saponin derived carbon dots with AIE properties for stable detection of HSA and extremely acidic pH

Shengtao Zhang^{a,b,§}, Bin Li^{b,§}, Jieyu Zhou^b, Jiayi Shi^b, Zhongjing He^b, Yumin Zhao^b, Yan Li^{a,*}, Yehua Shen^{a,*}, Yongmin Zhang^{b,c}, Shaoping Wu^{b,*}

^a Key Laboratory of Synthetic and Natural Functional Molecule Chemistry of the Ministry of Education, College of Chemistry and Materials Science, Northwest University, Xi'an, 710069, China.

^b School of Pharmacy, Key Laboratory of Resource Biology and Biotechnology in Western China, Ministry of Education, Biomedicine Key Laboratory of Shaanxi Province, Northwest University, 229 Taibai Road, Xi'an, Shaanxi, 710069, P. R. China.

^c Sorbonne Université, CNRS, Institut Parisien de Chimie Moléculaire, UMR 8232, 4 place Jussieu, 75005, Paris, France.

[§] These authors contributed equally to this work.

* Lead corresponding author: wushaoping@nwu.edu.cn

ABSTRACT

In this work, tea saponin (TS) which is indispensable in Camellia oleifera industry was used to synthesize a class of hydrophobic carbon dots (TS-CDs) with aggregation-induced emission (AIE) properties. A new fluorescent sensing platform based on AIE and non-modified TS-CDs for the detection of human serum albumin (HSA) and pH was developed, respectively. Interestingly, the developed platform is capable of ratiometric detecting extremely acidic pH in the range of 0.2-1.8 linearly ($R^2=0.9959$) due to protonation-deprotonation. Meanwhile, TS-CDs exhibited well stability toward HSA detection over a wide linear range (0~180 μ M), long-term (48 h), and wide pH range (2~13). Furthermore, TS-CDs was utilized to localize to mitochondria and detect HSA in living cells, demonstrating its promising perspective in biosensing applications. This work may pave a novel avenue for high value-added utilization in the extraction process of extracting camellia oil for food woody oil.

Keywords: Tea saponin; Carbon dots; AIE; HSA; pH; Mitochondria localization; Cell imaging.

Introduction

Carbon dots (CDs) are zero-dimensional materials with extremely small size, generally less than 10 nm in diameter (Xu et al., 2020). A large number of functional groups on the surface of carbon dots (such as hydroxyl, carboxyl, amino, etc.) enable CDs to be easy to functionalize (Alas et al., 2020). Due to excellent optical properties, such as excitation-dependent, up-converted luminescence, high resistance to photobleaching and photo-blinking, CDs were applied in many fields, such as biosensing (Zhu et al., 2013), anti-counterfeiting (Qu et al., 2012), drug transport (Panwar et al., 2019), super capacitor (Guo et al., 2022) etc.. Many fluorescent sensors based on CDs were reported to detect analytes such as vitamins (Luo et al., 2018), metal ions (He et al., 2020), amino acids (Lu et al., 2018), selenol (Wang et al., 2017). Certainly, accurate, timely and stable detection of signal molecules in living organisms is of great significance for studying activities in living organisms and diagnosing diseases in early stage. The sensing platform including “turn-off”, “turn-on”, “on-off-on” and “ratiometric” mode, in which “turn-on” and “ratiometric” probes can improve accuracy and suffer less background interference. Recently, researchers construct a ratiometric sensing platform based on neutral red and urea to detect L-Lysine and pH in living cells (Chang et al., 2022). Although there are many carbon dots used for biosensing, it’s still an important issue to develop multi-functional carbon dots with “turn-on” and ratiometric mode. Fluorescence of conventional probes will be quenched by aggregation due to π - π stacking effects which restricted their application. Therefore, Tang’s group in 2001 reported Aggregation induced emission (AIE) effect that realized solid state fluorescence through inhibiting intramolecular rotation or vibration (Luo et al., 2001). CDs with AIE properties were firstly synthesized by modifying polymer long-chain on the surface of CDs (Gao et al., 2013). Since then, AIE properties of carbon dots were synthesized by researchers through surface passivation which requires post-modification and the fluorescence may be quenched at high concentration. Therefore, it’s still a challenge to synthesis carbon dots with AIE properties without surface passivation (Arshad et al. 2021; Yang

et al., 2019).

HSA and pH are two important indicators related to human physiological activities. Unusual level of HSA is highly relative to diabetes and liver diseases (Murch et al., 1996). On the other hand, pH is related to various physiological activities (Shangguan et al., 2016). In recent years, many fluorescent probes for HSA and pH detection have been reported (J.-F. Xu et al., 2022; Li et al., 2020; Liu et al., 2022; Ning et al., 2018). However, most of the conventional dyes need to be ready-to-assay and cannot be stored for a long time, thus it makes sense to develop probes with good detection stability. Moreover, to the best of our knowledge, there is no probe that can detect pH values up to 0.2, and there are few probes that can detect HSA in a wide pH range and after long-term storage. Therefore, it is still necessary to achieve stable detection of HSA and detection of extremely acidic pH.

Camellia oleifera is one of the four major woody oilseeds in the world and well applied in edible oil industry, however, the utilization rate of oil residue after oil extraction is very low. The oil residue contains 10-15% tea saponin (TS), which is a natural surfactant that mixed of oleanane-type pentacyclic triterpenoid saponins was usually used as soap, ponding agent, etc. (Feng et al., 2015). There is little research has been demonstrated on the deep application of tea saponin (Kuo et al., 2010). Herein, we first used TS as raw material to synthesize a new class of carbon dots (TS-CDs) with the properties of AIE and pH responsive. TS-CDs was prepared by a solvothermal method without any surface modification or heteroatom doping. Moreover, TS-CDs has two fluorescence emission peaks at 313 nm and 533 nm with the properties of excitation-dependent and excitation-independent, respectively. Surprisingly, TS-CDs can bind to HSA through hydrophobic interaction and realize the detection of HSA by AIE and solvent effect. TS-CDs can also detect extremely acidic pH ratiometrically through protonation-deprotonation of TS-CDs. Compared with previous studies, TS-CDs has the advantages as follows: (1) Simple and economical synthesis of multifunctional CDs with a high quantum yield of 46.6%. (2) TS-CDs can stably detect HSA between pH 2~13 and the fluorescence intensity can

remain unchanged for 48 hours after adding HSA, label-free HSA imaging at cellular levels with low cytotoxicity can also be achieved. (3) Ratiometric and rapid detection of pH in extremely acidic conditions can be achieved.

2. Experimental

2.1. Materials and instruments

All the reagents were of analytical grade, purchased from Sinopharm Group. Tea saponin, amino acids, simvastatin were obtained from Energy-Chemical. Bodipy493/503 and mitochondrial red obtained from Tokyo Chemical Industry Co., Ltd. and Beyotime Biotechnology, respectively. All proteins were purchased from Shanghai McLean Biochemical Technology Co., Ltd. Dansyl-L-proline was purchased from Shanghai Aladdin Biochemical Technology Co., Ltd..

Transmission electron microscopy (TEM) and high-resolution TEM images were acquired from field emission transmission electron microscopy (Talos F200X). X-ray diffractometer (Bruker, Germany) was utilized to obtain X-ray powder diffraction (XRD) patterns. Tensor 27 FT-IR spectrometer (Bruker, Germany) was used to obtain Fourier transform infrared (FT-IR) spectra. X-ray photoelectron spectroscopy (XPS) was carried out with ESCALAB Xi+ (Thermo Scientific). Hitachi F-7000 was used to measure fluorescence spectra. UV Absorption Spectroscopy were recorded using a Shimadzu UV-1800 spectrophotometer. The pH was measured through a Sartorius PB-10 pH meter. Leica TCS SP8 confocal laser scanning microscope filmed the fluorescence imaging. Zeta potential was analyzed using a British Malvern Zetasizer Nano ZS. Toxicity experiments was carried out by Beijing Liuyi's WD-2102A.

2.2. Synthesis of TS-CDs

Tea sapogenin was synthesized with minor adjustments according to the literature of Kuo's group (Kuo et al., 2010). Tea saponin (0.50 g) was added to H₂O (12 mL) containing concentrated sulfuric acid (0.60 mL), then the solution was transferred into a 50 mL round-bottomed flask. The reaction was carried out at 100°C

for 5 h, then the raw materials were removed by filtration, tea sapogenin was extracted with ethyl acetate, 212 mg mixed sapogenin was obtained after vacuum drying. Concentrated hydrochloric acid (50 μ L) was added to the tea sapogenin (55 mg) in ethanol (10 mL). After the solution was heated at 230°C in a 25 mL Teflon autoclave for 6 h, a red-brown solution was obtained, then silica gel column chromatography was performed with dichloromethane as eluent to obtain TS-CDs, finally, 2.7 mg TS-CDs could be obtained after vacuum drying.

2.3. Calculation of fluorescence quantum yield

The method for calculating the fluorescence quantum yield of TS-CD was with reference to Wu's group (She et al., 2017), and the method is documented in the Supporting Information.

2.4. Fluorescence determination of HSA and pH

Phosphate buffer solution (PBS) was selected as the stabilizer to perform titration of HSA and pH. For the detection of HSA, different concentrations of HSA (0~180 μ M) were added into 200 μ L of TS-CDs (0.20 mg/mL) acetone solution in 15 mL colorimetric tube, after adding 500 μ L of PBS and diluting to 5.0 mL with water for 5 min, the fluorescence spectra were recorded at excitation wavelength of 380 nm. Under the same condition, selectivity and competition tests were carried out by adding the following proteins and amino acids including Bovine serum albumin (BSA), Homocysteine (Hcy), Glutathione (GSH), Cysteine (Cys), Leucine (Leu), Glu, Ascorbic acid (ASA), Valine (Val), Methionine (Met), Isoleucine (Ile), Serine (Ser), Arginine (Arg), Tryptophan (Trp), Threonine (Thr), Asparagine (Asn), Tyrosine (Tyr), Glycine (Gly), Alanine (Ala), Lysine (Lys), HGB (Hemoglobin), Papain, Pepsin, Chymotrypsin instead of HSA. Furthermore, some ions including Na^+ , Zn^{2+} , Mg^{2+} , K^+ , Hg^{2+} , Fe^{3+} , Fe^{2+} , Cu^{2+} , Ca^{2+} , Al^{3+} , ClO^- , F^- , I^- , NO_3^- , H_2O_2 , CO_3^{2-} , Cl^- , SO_4^{2-} , S^{2-} , SO_3^{2-} , HSO_3^- , $\text{S}_2\text{O}_3^{2-}$ were also used to check the selectivity and competition of TS-CDs.

For the detection of pH, 2.8 mL of 70% PBS solution with various pH was added to 200 μ L of TS-CDs (0.20 mg/mL) acetone solution and the fluorescence spectra

were measured at the excitation wavelength of 380 nm.

2.5. Bioimaging

Bioimaging experiments in HepG2 cells were with reference to (Ke et al., 2022; Ning et al., 2018), and the method was recorded completely in the Supporting Information.

3. Results and discussion

3.1. Characterization of TS-CDs

The structure and optical properties of TS-CDs were characterized by TEM, XRD, XPS, FT-IR, UV-Vis, FS. The lattice and size of TS-CDs were performed by TEM and HR-TEM images. As shown in Fig. 1A, TEM image and HR-TEM image of TS-CDs demonstrated near spherical structure and particle size of 2.5 ± 1 nm (The particle size statistical distribution curve was drawn used more than 100 particles). HR-TEM shows a 0.34 nm lattice spacing, which corresponds to (002) planes of bulk graphite. Similarly, XRD spectra (Fig. 1B) show a broad peak at 23° corresponding to the d-spacing value of around 0.34 nm. XPS was recorded to characterize surface elements of TS-CDs, the full survey scan (Fig. 1C) indicates that TS-CDs is mainly composed of carbon and oxygen. The HR-XPS C1s spectra (Fig. S1A) displays the existence of C-C or C=C (284.8 eV), -COOR (285.5 eV) and C-O (286.2 eV). HR-XPS O1s spectra (Fig. S1B) show the existence of C-O-C (533.8 eV) and C-O/C=O (532.5 eV). The functional groups of TS-CDs were analyzed by FT-IR, as the Fig. 1D shows, the peak of TS-CDs at 3437 cm^{-1} is caused by the stretching vibrations of O-H/N-H. The peaks at 2954 cm^{-1} and 2854 cm^{-1} are caused by symmetric and asymmetric stretching vibrations of -CH_3 , respectively. The scissor, symmetric and asymmetric stretching vibrations of saturated methylene are located at 1460 cm^{-1} , 2854 cm^{-1} and 2928 cm^{-1} , respectively. The peaks at 1637 cm^{-1} and 1460 cm^{-1} are generated by the stretching vibrations of C=C and C-N.

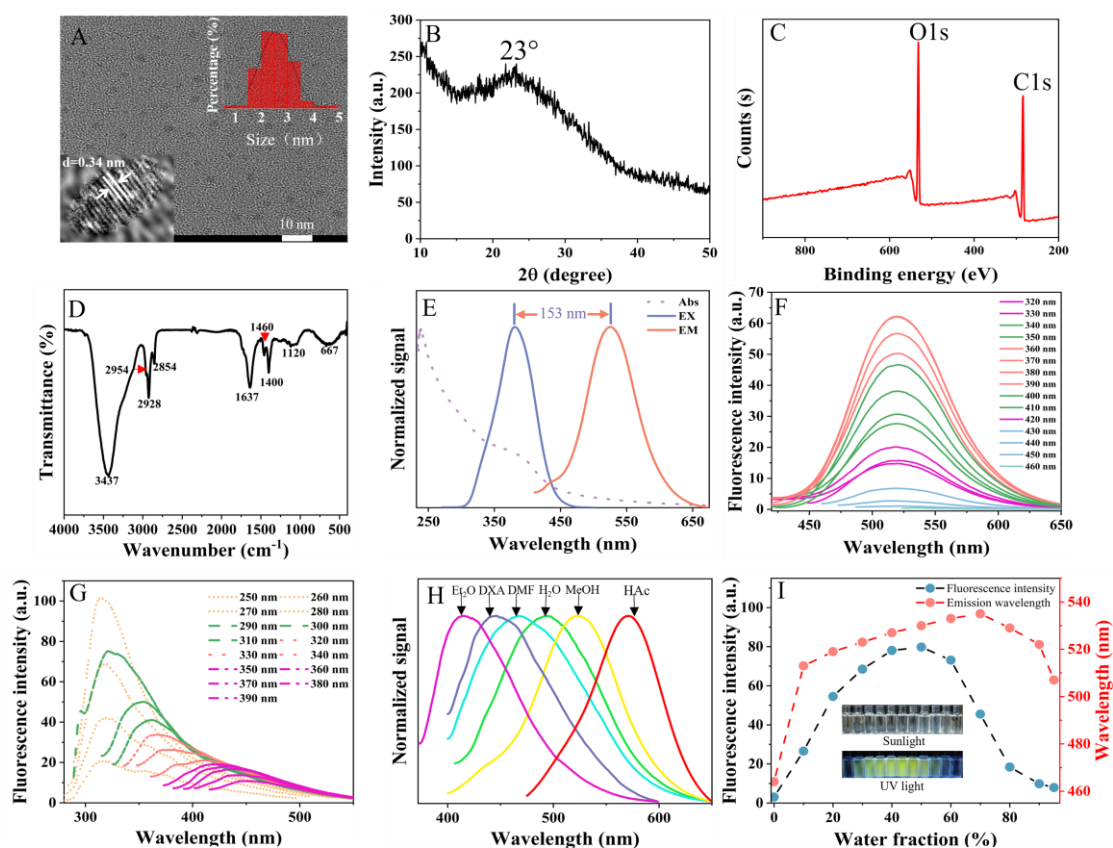


Fig. 1. (A) TEM image of TS-CDs, inset: particle size distribution image of TS-CDs (top right), HR-TEM image of TS-CDs (bottom left). (B) XRD spectra of TS-CDs (C) XPS spectrum of TS-CDs. (D) FT-IR spectrum of TS-CDs. (E) UV absorption spectra (purple line), fluorescence excitation spectra (blue line, $\lambda_{em}=533$ nm) and PL emission spectra (red line, $\lambda_{ex}=380$ nm) of TS-CDs. (F). Fluorescence spectra of TS-CDs in acetone (DMK) under different excitation wavelength (250 nm to 380 nm). (G). Fluorescence spectra of TS-CDs in MeOH under various excitation wavelength (320 nm to 460 nm). (H). Fluorescence emission ($\lambda_{ex}=380$ nm) spectra of TS-CDs in solvents with different polarity (from left to right are Ethyl ether (Et_2O), 1,4-Dioxane (DXA), N,N-Dimethylformamide (DMF), Water (H_2O), Methanol (MeOH), Acetic acid (HAc)). (I) Fluorescence emission intensity ($\lambda_{ex}=380$ nm) and fluorescence wavelength trend graphs of TS-CDs at different water fraction (0% to 90%), inset: photographs of TS-CDs with different water fraction (0% to 90%) under sunlight (above) and UV light (down).

3.2. Optical properties of TS-CDs

The optical properties of TS-CDs were characterized by UV-Vis and FS, As shown in Fig. 1E, the absorption peak at 237 nm belongs to the $\pi-\pi^*$ transition of C=C, and another characteristic band at 380 nm is from $n-\pi^*$ transition of C=N/C=O. The maximum excitation and emission wavelengths of TS-CDs in methanol are 380 nm and 533 nm, respectively, which corresponding to a large Stokes shift of 153 nm. The

maximum emission wavelength under acidic conditions is 593 nm and the Stokes shift reaches 213 nm (Fig. S2). Additionally, the fluorescence spectra of TS-CDs in acetone and MeOH were also collected as shown in Fig. 1F and 1G, emission peaks at 313 nm and 533 nm with excitation-dependent and excitation-independent feature respectively were investigated. As previously reported in the literature, the maximum emission peak at 313 nm with excitation-dependent belongs to classical luminescence of graphitic carbon cores, and the emission peak at 533 nm belongs to the luminescence of surface states of carbon dots (H. Yang et al., 2019).

The fluorescence spectra of TS-CDs in different polar solvents were also studied to explore its optical properties. As shown in Fig. 1H, the fluorescence peaks among 410 nm to 593 nm of TS-CDs were recorded in various solvents, and the fluorescence emission wavelength of TS-CDs gradually red-shifted with the increasing of polarity. Correspondingly, the red-shift trend of the UV absorption of TS-CDs in different solvents is consistent with the trend of the fluorescence spectrum was recorded in Fig. S3A. Fig. S3B is the photo of TS-CDs in different solvents under UV light and sun light, which shows the same trend as the fluorescence plot. TS-CDs shows blue fluorescence in solvents with less polar like DMK and yellow fluorescence in MeOH, while when the polarity continues to increase to that of acetonitrile and water, the fluorescence turns green due to the strong hydrophobicity of TS-CDs resulting in poor solubility and aggregated in water. The fluorescence peak of TS-CDs in acetic acid is only one at 593 nm, which is caused by the doping nitrogen protonation of TS-CDs carbon nuclei under acidic conditions (Xia et al., 2019).

The fluorescence spectra of TS-CDs in solvents with different water fraction were recorded to study its AIE properties (Fig. S3C and Fig. 1I), TS-CDs emits blue fluorescence in good solvent and gradually decreases accompanied by gradually increases of the yellow-green fluorescence at 533 nm as the gradual addition of poor solvent water from 0% to 60%. Equally, the UV absorption longer than 380 nm of TS-CDs also red-shifted with the increase of water fraction (Fig. S3D). As the water fraction increased to 90%, the strong hydrophobicity of TS-CDs leads to the

formation of larger aggregates, which enhanced the π - π stacking effect and gradually decreased the fluorescence intensity (Qian et al., 2009; Zhang et al., 2022). Such experiment was performed as shown in Fig. S4A, it was seen that high concentrations of TS-CDs (1 mg/mL) at 90% water fraction resulted in a turbid state with weak fluorescence, while the control group in methanol showed no precipitation and bright fluorescence. The fluorescence spectra of TS-CDs in different MeOH fraction were recorded to verify this hypothesis. It can be seen from Fig. S4B, the fluorescence intensity of TS-CDs increased as the gradual addition of poor solvent MeOH from 0% to 99%. The differentiation with Fig. S3C may be caused by the good solubility of TS-CDs in MeOH, making it difficult to form large aggregates.

3.3. Detection of HSA

Since TS-CDs is highly hydrophobic and possesses aggregation-induced emission property, solvent effect, we speculate that TS-CDs can response to HSA and emission enhanced. Researchers had proved that the addition of HSA can reduces the polarity of the system and will inhibit the rotation or vibration of the fluorophore (Chakrabarty et al., 2007; Vijayakumar et al., 2019; Xu et al., 2016). The fluorescence of TS-CDs increases with the addition of HSA due to the decreased of solvent polarity, which is consistent with the optical properties of TS-CDs that fluorescence intensity increased as the water fraction decreased from 90% to 60%. As designed, we performed experiments of TS-CDs in response to different proteins, amino acids, and ions, and found that the fluorescence intensity was enhanced only when HSA and bovine serum albumin (BSA) were added. TS-CDs is a sensitive fluorescence nanoprobe to detect HSA, and the limit of detection of HSA achieved 140 nM (Table. S1). As shown in Fig. 2A, with the concentration of HSA increased to 180 μ M, the fluorescence intensity of TS-CDs increased by 6.5 times with good linearity in both detection ranges of 6~70 μ M and 80~180 μ M, which R^2 reaches 0.9969 and 0.9972, respectively (Fig. 2B and C). We also studied the kinetic curve of TS-CDs-HSA (Fig. 2D). The fluorescence intensity of TS-CDs increased 7.7-fold at 10 s and reached a stable value at 6 min.

The stability of HSA detection was also studied. Initially, TS-CDs can stably detect HSA in the pH range of 2~13 (Fig. S5A). In addition, we investigated the ability of TS-CDs to resist ionic strength (demonstrated with NaCl). The fluorescence intensity of TS-CDs changed only very slightly at a concentration of 0.50 M and the intensity remained 83% at 1.0 M (Fig. S5B). Moreover, it was found in Fig. S5C that fluorescence intensity of TS-CDs-HSA remained after storage 48 h at room temperature which overcomes the disadvantages of traditional fluorescent dyes with a short storage time, which proved that TS-CDs could be used to detect HSA stably. TS-CDs could stably detect HSA Compared with Moreover, some comparisons in terms of synthesis, biocompatibility and responsiveness between TS-CDs and previously probes used to detect HSA were shown in Table. S2.

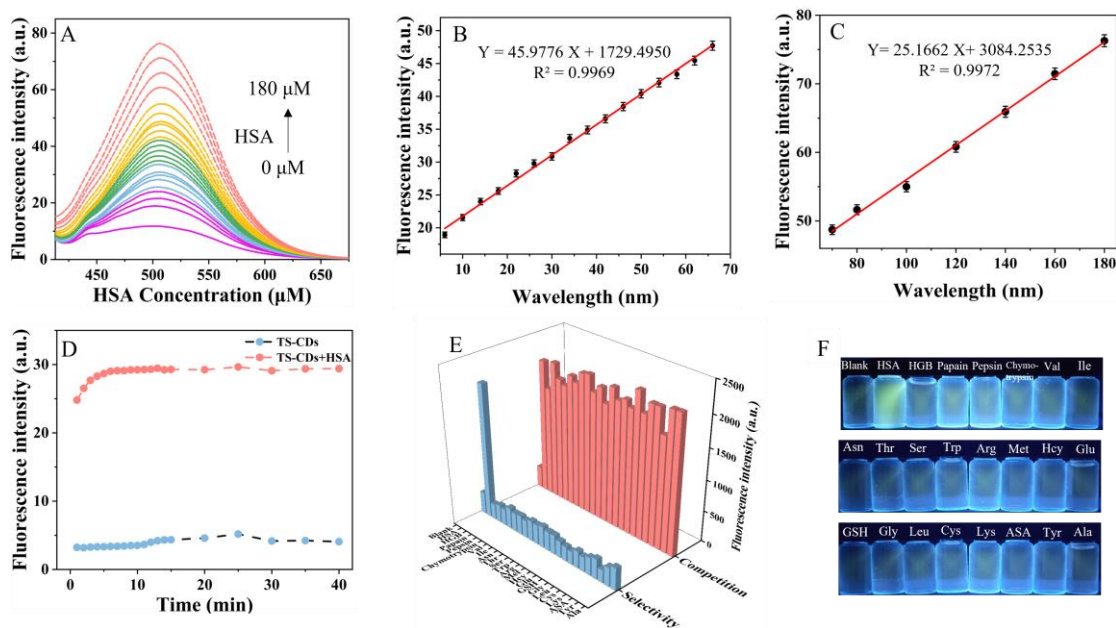


Fig. 2. (A) Fluorescence emission spectra ($\lambda_{\text{ex}}=380$ nm) of TS-CDs (8.0 $\mu\text{g/mL}$) upon addition of HSA (0~180 μM) in PBS (pH=7.4, containing 4% acetone) (B) Linear relationship of fluorescence emission ($\lambda_{\text{ex}}=380$ nm, $\lambda_{\text{em}}=505$ nm) and concentration of HSA (6~70 μM). (C) Linear relationship of fluorescence emission ($\lambda_{\text{ex}}=380$ nm, $\lambda_{\text{em}}=505$ nm) and concentration of HSA (70~180 μM). (D) Time course of fluorescence emission ($\lambda_{\text{ex}}=380$ nm, $\lambda_{\text{em}}=505$ nm) intensity graphs of TS-CDs in the absence (black line) and presence (red line) of HSA (70 μM) during 40 min. (E) Fluorescence emission intensity ($\lambda_{\text{ex}}=380$ nm, $\lambda_{\text{em}}=505$ nm) of TS-CDs (2.0 $\mu\text{g/mL}$, blue strips) and TS-CDs (2.0 $\mu\text{g/mL}$) + HSA (70 μM , red trips) in the presence of other proteins and amino acids. (F) Images of TS-CDs in the addition of other proteins and amino acids under 365 nm UV lamp.

Selective and competitive experiments were performed with proteins, amino

acids, anions, and cations against TS-CDs in PBS (pH 7.4). As shown in Fig. 2E, Under the same test conditions, Hcy, GSH, Cys, Leu, Glu, ASA, Val, Met, Ile, Ser, Arg, Trp, Thr, Asn, Tyr, Gly, Ala, Lys, BSA, HGB, Papain, Pepsin and Chymotrypsin that may co-exist with protein were used for selective and competitive experiments, only HSA among proteins, amino acids, anions, and cations had a largely enhanced fluorescence on making TS-CDs, probably because HSA can reduce the polarity of the system, while the other analytes cannot, the relative fluorescence spectrograms were shown in Fig. S6. Some anions and cations that Na^+ , Zn^{2+} , Mg^{2+} , K^+ , Hg^{2+} , Fe^{3+} , Fe^{2+} , Cu^{2+} , Ca^{2+} , Al^{3+} , ClO^- , F^- , I^- , NO_3^- , H_2O_2 , CO_3^{2-} , Cl^- , SO_4^{2-} , S^{2-} , SO_3^{2-} , HSO_3^- , $\text{S}_2\text{O}_3^{2-}$ also does not affect the detect of HSA (Fig. S7A). Competition experiments were also done for TS-CDs, the presence of other ions did not affect the response of TS-CDs to HSA (Fig. S7B). We also measured the response of TS-CDs to BSA, which is highly homologous to HSA, TS-CDs also respond to BSA (Fig. S8). However, BSA is not present in the human body, the response of TS-CDs to BSA does not affect the detection of HSA. These data indicate that TS-CDs have good selectivity for the detection of HSA.

3.4. Ratiometric detection of pH

Monitoring pH at different locations in human body is important to predict diseases and to understand the impact of pH on human health. Nowadays, there are many proposing probes for detecting pH (Yang et al., 2012), although only few places in human body in extremely acidic conditions, such as helicobacter pylori, microbiota in gastric juice, etc., highly sensitive probes that can stably detect extremely acidic pH are needed. The fluorescence intensity of TS-CDs upon the excitation wavelength of 380 nm varies greatly under extremely acidic conditions, but changes slowly when pH ≥ 2 which indicated that TS-CDs possess excellent stability that false positives could be avoided when detecting pH under extremely acidic conditions. The detection of pH on fluorescence emission intensity under an extremely acidic condition of 0.2~1.8 was recorded. It can be seen intuitively that the fluorescence intensity of TS-CDs at 593

nm decreased as pH increased from 0.2 to 1.8, on the contrary, the fluorescence intensity at 533 nm increased simultaneously (Fig. 3A). More importantly, a good linear relationship ($R^2=0.9959$) of $I_{533\text{ nm}}/I_{593\text{ nm}}$ could be observed from Fig. 3B, indicating that TS-CDs is highly pH sensitive. Moreover, the responses of TS-CDs to pH from 0.2-1.8 were reversible during 5 cycle times as shown in Fig. S10. Therefore, TS-CDs can be used to detect pH under extremely acidic conditions. From Fig. 3D, the orange fluorescence of TS-CDs was gradually weakened, and the yellow-green fluorescence increased with the pH increasing, which is consistent with the changes in the fluorescence picture.

To clarify the mechanism of TS-CDs responds to pH, the UV-Vis, FT-IR and zeta potential under different pH were studied. Fig. 3E is the UV absorption spectra of TS-CDs at pH 1.0 and pH 7.0, the UV absorption at 380 nm decreased slightly with the decrease of pH accompanied by a broadening of the absorption peak, which is the result of the widening of the particle size distribution due to the smaller particle size of the TS-CDs fraction under acidic conditions. Moreover, it combined with a red-shift of the UV absorption peak at 380 nm, corresponding to fluorescence spectra, the nitrogen is protonated due to both the edge/surface groups and the rigid carbon core structure under acidic conditions (Yuan et al., 2015). With the enhancement of alkalinity, the fluorescence at 593 nm decreases due to the doped nitrogen being deprotonated first, while the fluorescence enhancement at 533 nm is caused by the enhancement of van der Waals forces between carbon dots because of the deprotonation of edge/surface groups, followed by the aggregation of carbon dots. (Yang et al., 2020). The FT-IR absorption maps of TS-CDs at different pH were also investigated, as shown in Fig. 3F, the peak near 3400 cm^{-1} becomes weaker as the pH increases from 1.0 to 7.0, which is due to the weakening of the intensity of N-H and O-H caused by the deprotonation of carbon sites, and the -OH/-NH₂ peak is red-shifted from 3419 cm^{-1} to 3437 cm^{-1} as the pH increases from 1.0 to 7.0, which is a result of the enhanced of hydrogen bonds between TS-CDs hydroxyl groups (Song et al., 2016). Zeta potential of TS-CDs was investigated to explore the reason for the

aggregation of TS-CDs, as shown in Table S3, zeta potential value of TS-CDs was -4.43 mV at pH 7.0, which demonstrated that the surface of TS-CDs is negatively charged. As pH of TS-CDs decreased to 0.5, the zeta potential value achieved 2.97 mV by protonation of the surface groups of TS-CDs as the pH decreased. The zeta potential of TS-CDs increased sharply as the pH of TS-CDs increased from 7.0 to 12.0, which indicated that the -OH/O=C-NH₂/NH₂ of TS-CDs were depleted by deprotonation (Dan et al., 2021). Moreover, corresponding to the infrared absorption spectra, the stretching vibration of -OH/-NH₂ sharply decreased when the pH increased to 7.0. Based on the above observations, we concluded that TS-CDs has better solubility at acidic solutions and poor solubility in alkaline solutions.

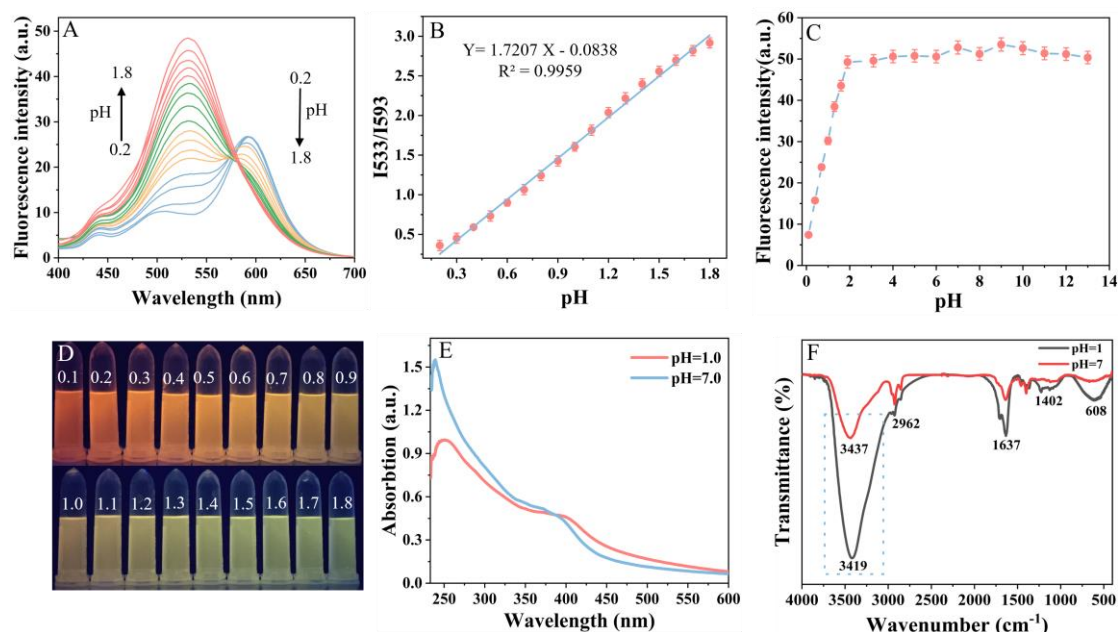


Fig. 3. (A) Fluorescence emission spectra of TS-CDs (8.0 µg/mL) (30% acetone and 70% water) at different pH (0.2~1.8) (B) Linear relationship of the fluorescence emission intensity (8.0 µg/mL) ratio of TS-CDs between 533 nm and 593 nm. (C) Changes in fluorescence emission intensity of TS-CDs (8.0 µg/mL, λ_{em} =533 nm) at different pH (0.1~13). (D) Images of TS-CDs at different pH (0.2~1.8) under UV-light (365 nm). (E) UV absorption diagram of TS-CDs at pH=1.0 (red line) and pH=7.0 (blue line). (F) FT-IR spectra of TS-CDs at pH=1.0 (black line) and pH=7.0 (red line).

3.5.1. Mitochondrial targeting assay of TS-CDs

To determine the intracellular localization of TS-CDs, we performed fluorescence co-localization experiments by using commercial Mito-tracker red and TS-CDs in HepG2 cells, as shown in Fig. 4A. There is a large overlap between the

green channel of TS-CDs fluorescence and the red channel of Mito-tracker red (Pearson correlation coefficient of 0.94), and by intensity cross-sectional analysis can be seen that the two peaks overlap well (Fig. 4B). In addition, the Pearson correlation coefficient was only 0.75 when using the lipid titration dye BODIPY 493/505 for co-localization experiments with TS-CDs (Fig. 4C), which clearly indicates that TS-CDs can target mitochondria.

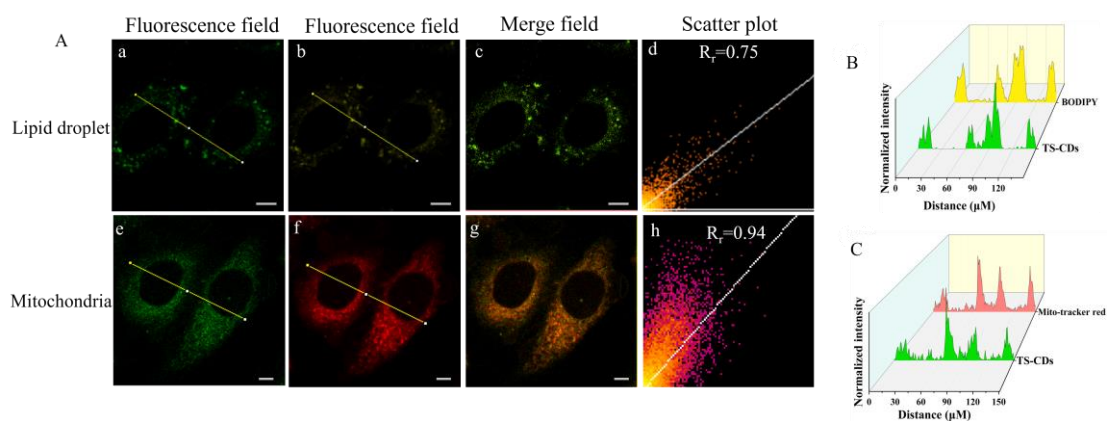
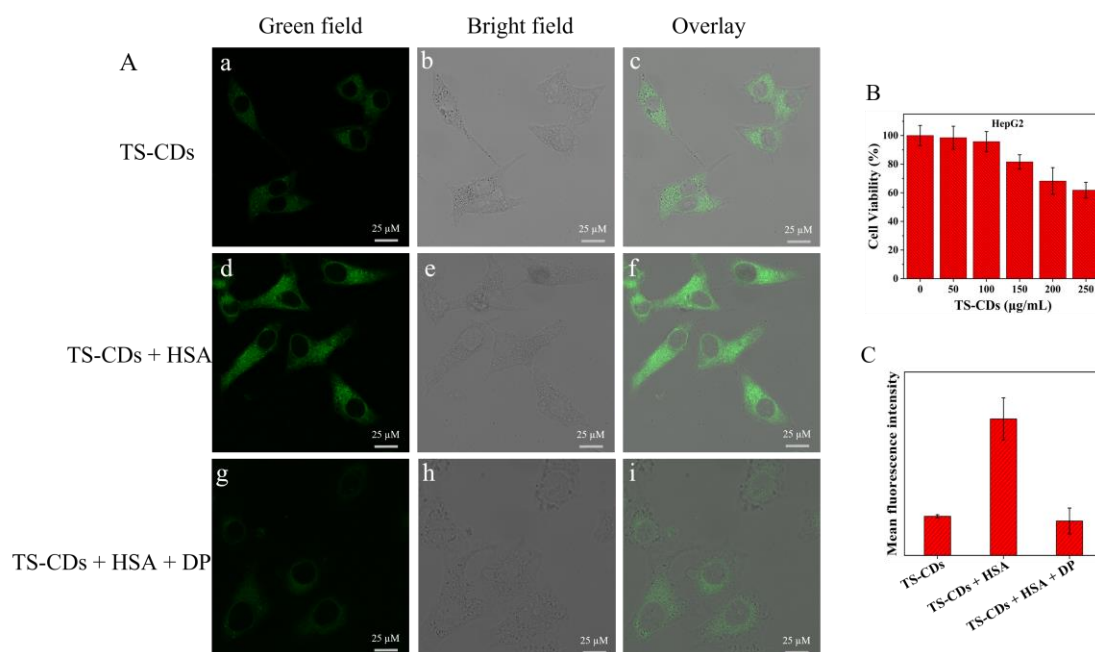


Fig. 4. (A) Confocal images of HepG2 cells. (a-c) Co-localization images of HepG2 cells after adding TS-CDs (8.0 $\mu\text{g/mL}$) and BODIPY 493/503 (0.5 μM) for 30 min. (d) Co-localization scatter plot of TS-CDs (8.0 $\mu\text{g/mL}$) and BODIPY 493/503 (1.0 μM). (e-g) Co-localization images of HepG2 cells incubated with TS-CDs (8.0 $\mu\text{g/mL}$) and Mito-tracker red (1.0 μM) for 30 min. (h) Co-localization scatter plot of TS-CDs (8.0 $\mu\text{g/mL}$) and Mito-tracker red. (B) Fluorescence intensity distribution of selected areas of a and b channels. (C) Fluorescence intensity distribution of selected areas of e and f channels. (a) and (e) The wavelength setting range is 480 nm to 530 nm for TS-CDs ($\lambda_{\text{ex}} = 380$ nm). (b) The wavelength setting range is 530 nm to 560 nm for BODIPY 493/503. (f) The wavelength setting range is 560 nm to 630 nm for Mito-tracker red ($\lambda_{\text{ex}} = 579$ nm).

3.5.2. Cell imaging of exogenous HSA

For probes used for biological imaging, good biocompatibility is acquired, especially for intracellular detection. Therefore, we first performed MTT experiments using HepG2 to examine the cytotoxicity of TS-CD. Fig. 5B shows the viability of HepG2 cells with TS-CDs concentration of 0~250 $\mu\text{g/mL}$, this test concentration is much higher than the fluorescence test concentration of 8.0 $\mu\text{g/mL}$, the viability of 150 $\mu\text{g/mL}$ in TS-CDs can be seen higher than 90%, indicating that TS-CDs has less cytotoxicity. Fig. 5A (a-c) shows that HepG2 cells co-incubated with TS-CDs (8.0

374 $\mu\text{g/mL}$) for 30 minutes in the green channel showed only weak fluorescence. In
 375 contrast, bright green fluorescence was observed after incubation with HSA ($70.0 \mu\text{M}$)
 376 for 24 hours followed by TS-CD ($8.0 \mu\text{g/mL}$) for 30 minutes (Fig. 5A, d-f). Fig. 5A,
 377 (g-i) are the imaging pictures after adding HSA inhibitor Dansyl-L-proline (DP),
 378 whose fluorescence intensity was weaker than d-f. Fig. 5C from left to right shows the
 379 mean fluorescence intensity of HepG2 cells after incubation with TS-CDs, TS-CDs +
 380 HSA and TS-CDs + HSA + DP, respectively. These results indicated that TS-CDs can
 381 be used to image intracellular HSA.



382 **Fig. 5.** (A) Confocal images of HepG2 cells after incubated with TS-CDs ($8.0 \mu\text{g/mL}$) for 30
 383 min(a-c), TS-CDs ($8.0 \mu\text{g/mL}$) for 30 min and HSA ($70 \mu\text{M}$) for 24 h (d-f). HSA ($70 \mu\text{M}$) for 24 h,
 385 DP (3.0 mM) for 30 min and TS-CDs ($8.0 \mu\text{g/mL}$) for 30 min (g-i). (B) Cell viability of HepG2
 386 cells after incubated with TS-CDs (0~250 $\mu\text{g/mL}$). (C) Mean fluorescence intensity of TS-CDs,
 387 TS-CDs + HSA and TS-CDs + HSA + DP.

388 3.5.3. Drug-induced cell imaging of HSA

389 HSA levels are often associated with drug and toxic substance assessments. We
 390 used simvastatin (a drug used for rising content of HSA) to stimulate HepG2 cells to
 391 produce HSA (Ha et al., 2009). As shown in Fig. 6A (a-c), after incubation with
 392 simvastatin ($1.0 \mu\text{M}$) for 24 hours and then with TS-CD for 30 minutes, the
 393 fluorescence intensity was significantly enhanced. However, the control group to
 394 which the simvastatin inhibitor DP (3.0 mM) was added showed weaker fluorescence

Fig. 6A (d-f) (Wang et al., 2017). The above experiments show that TS-CDs can penetrate cell membranes and have the ability to detect intracellular HSA levels.

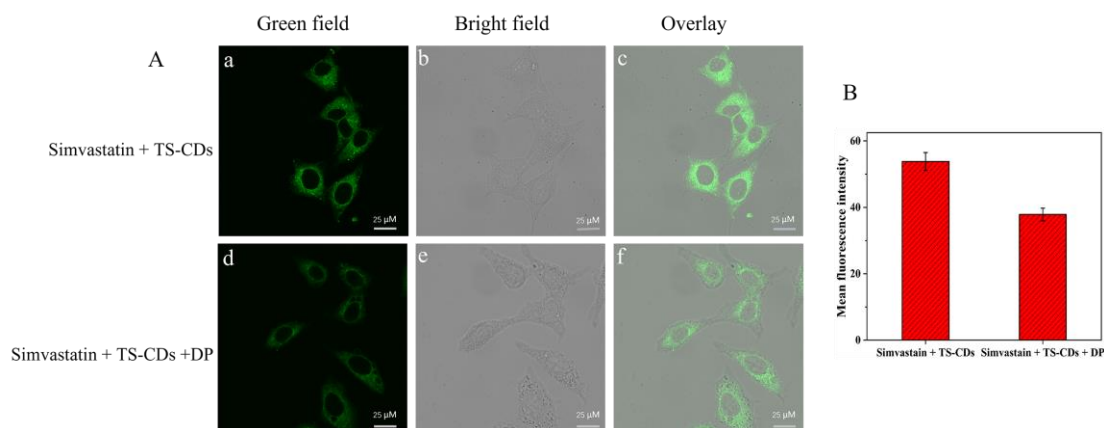


Fig. 6. (A) Confocal images of HepG2 cells after incubated with simvastatin (1.0 μM) for 24 h and TS-CDs (8.0 μg/mL) for 30 min (a-c). Simvastatin (1 μM) for 24 h and TS-CDs (8.0 μg/mL) for 30 min, DP (3.0 mM) for 30 min (d-f) (B) Mean fluorescence intensity of simvastatin +TS-CDs and simvastatin + TS-CDs + DP.

4. Conclusion

In summary, we synthesized a multifunctional hydrophobic TS-CDs by a simple solvothermal method using tea saponin as raw material. The synthesized TS-CDs has strong hydrophobicity, AIE properties, solvent effect and double emission at 313 nm and 533 nm, respectively. Results indicated that TS-CDs can be applied as a sensing platform for the detection of HSA due to AIE property and pH under extremely acidic condition (0.2-1.8). Due to the use of natural product as carbon source, the synthesized TS-CDs has good biocompatibility that can stably detect HSA in a wide pH range (2-13) and a long time (48 h), and this probe could be applied to visualize the concentration of HSA in living cells. Moreover, the ratiometric detection of pH under extremely acidic conditions (0.2-1.8) was also realized due to protonation – deprotonation of TS-CDs. The current work demonstrates that the synthesis and biological applications of TS-CDs may pave a novel avenue for high value-added utilization in the extraction process of extracting camellia oil for food woody oil. This strategy could be easily extended to detection other disease-related biomarker proteins.

Acknowledgements

The authors thank the National Key Research and Development Project of China (2019YFD1002400), the National Natural Science Foundation of China (No. 22074119), the International Science & Technology Cooperation Program of Shaanxi Province (No. 2019KWZ-001), Biomedicine Key Laboratory of Shaanxi Province (No. 2018SZS41).

References

- Alas, M. O., Alkas, F. B., Aktas Sukuroglu, A., Genc Alturk, R., & Battal, D. (2020). Fluorescent carbon dots are the new quantum dots: an overview of their potential in emerging technologies and nanosafety. *Journal of Materials Science*, 55(31), 15074-15105. doi:10.1007/s10853-020-05054-y
- Arshad, F., Pal, A., & Sk, M. P. (2021). Review—aggregation-induced emission in carbon dots for potential Applications. *ECS Journal of Solid State Science and Technology*, 10(2). doi:10.1149/2162-8777/abdfb8
- Chakrabarty, A., Mallick, A., Haldar, B., Das, P., & Chattopadhyay, N. (2007). Binding interaction of a biological photosensitizer with serum albumins: a biophysical study. *Biomacromolecules*, 8(3), 920-927. doi:10.1021/bm061084s
- Chang, D., Zhao, Z., Shi, H., Feng, J., Yang, Y., & Shi, L. (2022). Ratiometric fluorescent carbon dots for enantioselective sensing of L-lysine and pH discrimination in vivo and in vitro. *Sensors and Actuators B: Chemical*, 362, 131792. doi:10.1016/j.snb.2022.131792
- Dan, C., Zhao, Z., Feng, J., Xin, Y., Yang, Y., & Shi, L. (2021). Lysosome-targeted red-fluorescent carbon dots for turn-on detection of permanganate and pH in vivo and in vitro. *Sensors and Actuators B: Chemical*, 349, 130774. doi:10.1016/j.snb.2021.130774
- Feng, J., Chen, Y., Liu, X., & Liu, S. (2015). Efficient improvement of surface activity of tea saponin through Gemini-like modification by straightforward esterification. *Food Chemistry*, 171, 272-279. doi:10.1016/j.foodchem.2014.08.125
- Gao, M. X., Liu, C. F., Wu, Z. L., Zeng, Q. L., Yang, X. X., Wu, W. B., . . . Huang, C. Z. (2013). A surfactant-assisted redox hydrothermal route to prepare highly photoluminescent carbon quantum dots with aggregation-induced emission enhancement properties. *Chemical Communications (Camb)*, 49(73), 8015-8017. doi:10.1039/c3cc44624g
- Guo, J., Lu, Y., Xie, A. Q., Li, G., Liang, Z. B., Wang, C. F., . . . Chen, S. (2022). Yellow-emissive carbon dots with high solid-state photoluminescence. *Advanced Functional Materials*, 32(20). doi:10.1002/adfm.202110393
- Ha, C. E., Ha, J. S., Theriault, A. G., & Bhagavan, N. V. (2009). Effects of statins on the secretion of human serum albumin in cultured HepG2 cells. *Journal of Biomedical Science*, 16, 32. doi:10.1186/1423-0127-16-32
- He, X., Han, Y., Luo, X., Yang, W., Li, C., Tang, W., . . . Li, Z. (2020). Terbium (III)-referenced N-doped carbon dots for ratiometric fluorescent sensing of mercury (II) in seafood. *Food Chemistry*, 320, 126624. doi:10.1016/j.foodchem.2020.126624
- Ke, Y., Cao, J., Gong, J., & Fu, N. (2022). A near-infrared naphthalimide fluorescent probe for targeting

- the lysosomes of liver cancer cells and specifically selecting HSA. *Sensors and Actuators B: Chemical*, 352, 131015. doi:10.1016/j.snb.2021.131015
- Kuo, P. C., Lin, T. C., Yang, C. W., Lin, C. L., Chen, G. F., & Huang, J. W. (2010). Bioactive saponin from tea seed pomace with inhibitory effects against *Rhizoctonia solani*. *Journal of Agricultural and Food Chemistry*, 58(15), 8618-8622. doi:10.1021/jf1017115
- Li, X., Feng, Q., Qu, L., Zhao, T., Li, X., Bai, T., . . . Li, J. (2020). A water-soluble and incubate-free fluorescent environment-sensitive probe for ultrafast visualization of protein thiols within living cells. *Analytica Chimica Acta*, 1126, 72-81. doi:10.1016/j.aca.2020.06.026
- Liu, Y., Yu, Y., Meng, Q., Wei, Q., He, W., Zhao, Q., . . . Zhang, J. (2022). A fluorescent pH probe for evaluating the freshness of chicken breast meat. *Food Chemistry*, 384, 132554. doi:10.1016/j.foodchem.2022.132554
- Lu, M., Duan, Y., Song, Y., Tan, J., & Zhou, L. (2018). Green preparation of versatile nitrogen-doped carbon quantum dots from watermelon juice for cell imaging, detection of Fe³⁺ ions and cysteine, and optical thermometry. *Journal of Molecular Liquids*, 269, 766-774. doi:10.1016/j.molliq.2018.08.101
- Luo, J., Xie, Z., Lam, J. W., Cheng, L., Chen, H., Qiu, C., . . . Tang, B. Z. (2001). Aggregation-induced emission of 1-methyl-1,2,3,4,5-pentaphenylsilole. *Chemical Communications (Camb)*(18), 1740-1741. doi:10.1039/b105159h
- Luo, X., Zhang, W., Han, Y., Chen, X., Zhu, L., Tang, W., . . . Li, Z. (2018). N,S co-doped carbon dots based fluorescent "on-off-on" sensor for determination of ascorbic acid in common fruits. *Food Chemistry*, 258, 214-221. doi:10.1016/j.foodchem.2018.03.032
- Murch, S. H., Phillips, D., Walker-Smith, J. A., Winyard, P. J. D., Meadows, N., Koletzko, S., . . . Klein, J. (1996). Congenital enterocyte heparan sulphate deficiency with massive albumin loss, secretory diarrhoea, and malnutrition. *The Lancet*, 347(9011), 1299-1301. doi:https://doi.org/10.1016/S0140-6736(96)90941-1
- Ning, Y., Cui, J., Lu, Y., Wang, X., Xiao, C., Wu, S., . . . Zhang, Y. (2018). De novo design and synthesis of a novel colorimetric fluorescent probe based on naphthalenone scaffold for selective detection of hypochlorite and its application in living cells. *Sensors and Actuators B: Chemical*, 269, 322-330. doi:10.1016/j.snb.2018.04.156
- Ning, Y., Wang, X., Sheng, K., Yang, L., Han, W., Xiao, C., . . . Wu, S. (2018). A novel colorimetric and fluorescence turn-on pH sensor with a notably large Stokes shift for its application. *New Journal of Chemistry*, 42(17), 14510-14516. doi:10.1039/c8nj02860e
- Panwar, N., Soehartono, A. M., Chan, K. K., Zeng, S., Xu, G., Qu, J., . . . Chen, X. (2019). Nanocarbons for biology and medicine: sensing, imaging, and drug delivery. *Chemical Reviews*, 119(16), 9559-9656. doi:10.1021/acs.chemrev.9b00099
- Qian, L., Tong, B., Shen, J., Shi, J., Zhi, J., Dong, Y., . . . Tang, B. Z. (2009). Crystallization-induced emission enhancement in a phosphorus-containing heterocyclic luminogen. *The Journal of Physical Chemistry B*, 113(27), 9098-9103. doi:10.1021/jp900665x
- Qu, S., Wang, X., Lu, Q., Liu, X., & Wang, L. (2012). A biocompatible fluorescent ink based on water-soluble luminescent carbon nanodots. *Angewandte Chemie International Edition*, 51(49), 12215-12218. doi:10.1002/anie.201206791
- Shangguan, J., He, D., He, X., Wang, K., Xu, F., Liu, J., . . . Huang, J. (2016). Label-free carbon-dots-based ratiometric fluorescence pH nanoprobe for intracellular pH sensing. *Analytical Chemistry*, 88(15), 7837-7843. doi:10.1021/acs.analchem.6b01932

- She, M., Wu, S., Wang, Z., Ma, S., Yang, Z., Yin, B., . . . Li, J. (2017). Exploration of congeneric Hg(II)-mediated chemosensors driven by S-Hg affinity, and their application in living system. *Sensors and Actuators B: Chemical*, 247, 129-138. doi:10.1016/j.snb.2017.03.015
- Song, Z., Quan, F., Xu, Y., Liu, M., Cui, L., & Liu, J. (2016). Multifunctional N,S co-doped carbon quantum dots with pH- and thermo-dependent switchable fluorescent properties and highly selective detection of glutathione. *Carbon*, 104, 169-178. doi:10.1016/j.carbon.2016.04.003
- Vijayakumar, C., Kartha, K. K., Balan, B., Poulose, S., & Takeuchi, M. (2019). Protein-assisted supramolecular control over fluorescence resonance energytransfer in aqueous medium. *The Journal of Physical Chemistry C*, 123(20), 13141-13146. doi:10.1021/acs.jpcc.9b02002
- Wang, G., Xu, W., Guo, Y., & Fu, N. (2017). Near-infrared squaraine dye as a selective protein sensor based on self-assembly. *Sensors and Actuators B: Chemical*, 245, 932-937. doi:10.1016/j.snb.2017.01.172
- Wang, Q., Zhang, S., Zhong, Y., Yang, X. F., Li, Z., & Li, H. (2017). Preparation of yellow-green-emissive carbon dots and their application in constructing a fluorescent turn-on nanoprobe for imaging of selenol in living cells. *Analytical Chemistry*, 89(3), 1734-1741. doi:10.1021/acs.analchem.6b03983
- Xia, C., Cao, M., Xia, J., Zhou, G., Jiang, D., Zhang, D., . . . Li, H. (2019). An ultrafast responsive and sensitive ratiometric fluorescent pH nanoprobe based on label-free dual-emission carbon dots. *Journal of Materials Chemistry C*, 7(9), 2563-2569. doi:10.1039/c8tc05693e
- Xu, D., Lin, Q., & Chang, H. T. (2020). Recent advances and sensing applications of carbon dots. *Small Methods*, 4(4). doi:10.1002/smt.201900387
- Xu, J.-F., Yang, Y.-S., Jiang, A.-Q., & Zhu, H.-L. (2022). Detection methods and research progress of human serum albumin. *Critical Reviews in Analytical Chemistry*, 52(1), 72-92. doi:10.1080/10408347.2020.1789835
- Xu, Z.-Q., Yang, Q.-Q., Lan, J.-Y., Zhang, J.-Q., Peng, W., Jin, J.-C., . . . Liu, Y. (2016). Interactions between carbon nanodots with human serum albumin and γ -globulins: The effects on the transportation function. *Journal of Hazardous Materials*, 301, 242-249. doi:https://doi.org/10.1016/j.jhazmat.2015.08.062
- Yang, H., Liu, Y., Guo, Z., Lei, B., Zhuang, J., Zhang, X., . . . Hu, C. (2019). Hydrophobic carbon dots with blue dispersed emission and red aggregation-induced emission. *Nature Communications*, 10(1), 1789. doi:10.1038/s41467-019-09830-6
- Yang, M., Song, Y., Zhang, M., Lin, S., Hao, Z., Liang, Y., . . . Chen, P. R. (2012). Converting a solvatochromic fluorophore into a protein-based pH indicator for extreme acidity. *Angewandte Chemie International Edition*, 51(31), 7674-7679. doi:10.1002/anie.201204029
- Yang, Y. Z., Xiao, N., Liu, S. G., Han, L., Li, N. B., & Luo, H. Q. (2020). pH-induced aggregation of hydrophilic carbon dots for fluorescence detection of acidic amino acid and intracellular pH imaging. *Materials Science & Engineering C-Materials for Biological Applications*, 108, 110401. doi:10.1016/j.msec.2019.110401
- Yuan, F., Ding, L., Li, Y., Li, X., Fan, L., Zhou, S., . . . Yang, S. (2015). Multicolor fluorescent graphene quantum dots colorimetrically responsive to all-pH and a wide temperature range. *Nanoscale*, 7(27), 11727-11733. doi:10.1039/c5nr02007g
- Zhang, F., Du, T., Jiang, L., Zhu, L., & Tian, D. (2022). A combined "AIE + ESIPT" fluorescent probe for detection of lipase activity. *Bioorganic Chemistry*, 128, 106026. doi:10.1016/j.bioorg.2022.106026

545 Zhu, S., Meng, Q., Wang, L., Zhang, J., Song, Y., Jin, H., . . . Yang, B. (2013). Highly
546 photoluminescent carbon dots for multicolor patterning, sensors, and bioimaging. *Angewandte*
547 *Chemie International Edition*, 52(14), 3953-3957. doi:10.1002/anie.201300519

548